EUROPEAN ORGANISATION FOR NUCLEAR RESEARCH

CERN-PPE/96-156
6th November 1996

Production of Fermion-pair Events in e^+e^- Collisions at 161 GeV Centre-of-mass Energy

The OPAL Collaboration

Abstract

Cross-sections for hadronic and leptonic two-fermion events, and leptonic forward-backward asymmetries, have been measured in e^+e^- collisions at a centre-of-mass energy of 161 GeV, using the OPAL detector at LEP. Results are presented both including and excluding the dominant production of radiative γZ^0 events. We have measured R_b, the ratio of the number of $b\bar{b}$ to all multihadronic events at 161 GeV, and compared it to the result obtained at 130–136 GeV. All results agree well with the Standard Model expectations. In a model-independent fit to the Z^0 lineshape, the data presented here give an improved precision on the γZ^0-interference term. The data have also been used to obtain new limits on extensions of the Standard Model described by effective four-fermion contact interactions.

Submitted to Physics Letters B

The OPAL Collaboration

K. Ackerstaff[8], G. Alexander[23], J. Allison[16], N. Altekamp[5], K. Ametewee[25], K.J. Anderson[9], S. Anderson[12], S. Arcelli[2], S. Asai[24], D. Axen[29], G. Azuelos[18,a], A.H. Ball[17], E. Barberio[8], R.J. Barlow[16], R. Bartoldus[3], J.R. Batley[5], J. Bechtluft[14], C. Beeston[16], T. Behnke[8], A.N. Bell[1], K.W. Bell[20], G. Bella[23], S. Bentvelsen[8], P. Berlich[10], S. Bethke[14], O. Biebel[14], V. Blobel[27], I.J. Bloodworth[1], J.E. Bloomer[1], M. Bobinski[10], P. Bock[11], H.M. Bosch[11], M. Boutemeur[34], B.T. Bouwens[12], S. Braibant[12], R.M. Brown[20], H.J. Burckhart[8], C. Burgard[8], R. Bürgin[10], P. Capiluppi[2], R.K. Carnegie[6], A.A. Carter[13], J.R. Carter[5], C.Y. Chang[17], D.G. Charlton[1,b], D. Chrisman[4], P.E.L. Clarke[15], I. Cohen[23], J.E. Conboy[15], O.C. Cooke[16], M. Cuffiani[2], S. Dado[22], C. Dallapiccola[17], G.M. Dallavalle[2], S. De Jong[12], L.A. del Pozo[8], K. Desch[3], M.S. Dixit[7], E. do Couto e Silva[12], M. Doucet[18], E. Duchovni[26], G. Duckeck[34], I.P. Duerdoth[16], J.E.G. Edwards[16], P.G. Estabrooks[6], H.G. Evans[9], M. Evans[13], F. Fabbri[2], P. Fath[11], F. Fiedler[27], M. Fierro[2], H.M. Fischer[3], R. Folman[26], D.G. Fong[17], M. Foucher[17], A. Fürtjes[8], P. Gagnon[7], J.W. Gary[4], J. Gascon[18], S.M. Gascon-Shotkin[17], N.I. Geddes[20], C. Geich-Gimbel[3], T. Geralis[20], G. Giacomelli[2], P. Giacomelli[4], R. Giacomelli[2], V. Gibson[5], W.R. Gibson[13], D.M. Gingrich[30,a], D. Glenzinski[9], J. Goldberg[22], M.J. Goodrick[5], W. Gorn[4], C. Grandi[2], E. Gross[26], J. Grunhaus[23] M. Gruwé[8], C. Hajdu[32], G.G. Hanson[12], M. Hansroul[8], M. Hapke[13], C.K. Hargrove[7], P.A. Hart[9], C. Hartmann[3], M. Hauschild[8], C.M. Hawkes[5], R. Hawkings[8], R.J. Hemingway[6], M. Herndon[17], G. Herten[10], R.D. Heuer[8], M.D. Hildreth[8], J.C. Hill[5], S.J. Hillier[1], T. Hilse[10], P.R. Hobson[25], R.J. Homer[1], A.K. Honma[28,a], D. Horváth[32,c], R. Howard[29], R.E. Hughes-Jones[16], D.E. Hutchcroft[5], P. Igo-Kemenes[11], D.C. Imrie[25], M.R. Ingram[16], K. Ishii[24], A. Jawahery[17], P.W. Jeffreys[20], H. Jeremie[18], M. Jimack[1], A. Joly[18], C.R. Jones[5], G. Jones[16], M. Jones[6], R.W.L. Jones[8], U. Jost[11], P. Jovanovic[1], T.R. Junk[8], D. Karlen[6], K. Kawagoe[24], T. Kawamoto[24], R.K. Keeler[28], R.G. Kellogg[17], B.W. Kennedy[20], B.J. King[8], J. Kirk[29], S. Kluth[8], T. Kobayashi[24], M. Kobel[10], D.S. Koetke[6], T.P. Kokott[3], M. Kolrep[10], S. Komamiya[24], T. Kress[11], P. Krieger[6], J. von Krogh[11], P. Kyberd[13], G.D. Lafferty[16], R. Lahmann[17], W.P. Lai[19], D. Lanske[14], J. Lauber[15], S.R. Lautenschlager[31], J.G. Layter[4], D. Lazic[22], A.M. Lee[31], E. Lefebvre[18], D. Lellouch[26], J. Letts[2], L. Levinson[26], C. Lewis[15], S.L. Lloyd[13], F.K. Loebinger[16], G.D. Long[17], M.J. Losty[7], J. Ludwig[10], M. Mannelli[8], S. Marcellini[2], C. Markus[3], A.J. Martin[13], J.P. Martin[18], G. Martinez[17], T. Mashimo[24], W. Matthews[25], P. Mättig[3], W.J. McDonald[30], J. McKenna[29], E.A. Mckigney[15], T.J. McMahon[1], A.I. McNab[13], R.A. McPherson[8], F. Meijers[8], S. Menke[3], F.S. Merritt[9], H. Mes[7], J. Meyer[27], A. Michelini[2], G. Mikenberg[26], D.J. Miller[15], R. Mir[26], W. Mohr[10], A. Montanari[2], T. Mori[24], M. Morii[24], U. Müller[3], K. Nagai[26], I. Nakamura[24], H.A. Neal[8], B. Nellen[3], B. Nijjhar[16], R. Nisius[8], S.W. O'Neale[1], F.G. Oakham[7], F. Odorici[2], H.O. Ogren[12], N.J. Oldershaw[16], T. Omori[24], M.J. Oreglia[9], S. Orito[24], J. Pálinkás[33,d], G. Pásztor[32], J.R. Pater[16], G.N. Patrick[20], J. Patt[10], M.J. Pearce[1], S. Petzold[27], P. Pfeifenschneider[14], J.E. Pilcher[9], J. Pinfold[30], D.E. Plane[8], P. Poffenberger[28], B. Poli[2], A. Posthaus[3], H. Przysiezniak[30], D.L. Rees[1], D. Rigby[1], S. Robertson[28], S.A. Robins[13], N. Rodning[30], J.M. Roney[28], A. Rooke[15], E. Ros[8], A.M. Rossi[2], M. Rosvick[28], P. Routenburg[30], Y. Rozen[22], K. Runge[10], O. Runolfsson[8], U. Ruppel[14], D.R. Rust[12], R. Rylko[25], K. Sachs[10], E.K.G. Sarkisyan[23], M. Sasaki[24], C. Sbarra[2], A.D. Schaile[34], O. Schaile[34], F. Scharf[3], P. Scharff-Hansen[8], P. Schenk[27], B. Schmitt[8], S. Schmitt[11], M. Schröder[8], H.C. Schultz-Coulon[10], M. Schulz[8], M. Schumacher[3], P. Schütz[3], W.G. Scott[20], T.G. Shears[16], B.C. Shen[4], C.H. Shepherd-Themistocleous[8], P. Sherwood[15], G.P. Siroli[2], A. Sittler[27],

A. Skillman[15], A. Skuja[17], A.M. Smith[8], T.J. Smith[28], G.A. Snow[17], R. Sobie[28], S. Söldner-Rembold[10], R.W. Springer[30], M. Sproston[20], A. Stahl[3], M. Steiert[11], K. Stephens[16], J. Steuerer[27], B. Stockhausen[3], D. Strom[19], F. Strumia[8], P. Szymanski[20], R. Tafirout[18], S.D. Talbot[1], S. Tanaka[24], P. Taras[18], S. Tarem[22], M. Thiergen[10], M.A. Thomson[8], E. von Törne[3], S. Towers[6], I. Trigger[18], T. Tsukamoto[24], E. Tsur[23], A.S. Turcot[9], M.F. Turner-Watson[8], P. Utzat[11], R. Van Kooten[12], M. Verzocchi[10], P. Vikas[18], M. Vincter[28], E.H. Vokurka[16], F. Wäckerle[10], A. Wagner[27], C.P. Ward[5], D.R. Ward[5], J.J. Ward[15], P.M. Watkins[1], A.T. Watson[1], N.K. Watson[7], P.S. Wells[8], N. Wermes[3], J.S. White[28], B. Wilkens[10], G.W. Wilson[27], J.A. Wilson[1], G. Wolf[26], S. Wotton[5], T.R. Wyatt[16], S.. Yamashita[24], G. Yekutieli[26], V. Zacek[18],

[1]School of Physics and Space Research, University of Birmingham, Birmingham B15 2TT, UK
[2]Dipartimento di Fisica dell' Università di Bologna and INFN, I-40126 Bologna, Italy
[3]Physikalisches Institut, Universität Bonn, D-53115 Bonn, Germany
[4]Department of Physics, University of California, Riverside CA 92521, USA
[5]Cavendish Laboratory, Cambridge CB3 0HE, UK
[6] Ottawa-Carleton Institute for Physics, Department of Physics, Carleton University, Ottawa, Ontario K1S 5B6, Canada
[7]Centre for Research in Particle Physics, Carleton University, Ottawa, Ontario K1S 5B6, Canada
[8]CERN, European Organisation for Particle Physics, CH-1211 Geneva 23, Switzerland
[9]Enrico Fermi Institute and Department of Physics, University of Chicago, Chicago IL 60637, USA
[10]Fakultät für Physik, Albert Ludwigs Universität, D-79104 Freiburg, Germany
[11]Physikalisches Institut, Universität Heidelberg, D-69120 Heidelberg, Germany
[12]Indiana University, Department of Physics, Swain Hall West 117, Bloomington IN 47405, USA
[13]Queen Mary and Westfield College, University of London, London E1 4NS, UK
[14]Technische Hochschule Aachen, III Physikalisches Institut, Sommerfeldstrasse 26-28, D-52056 Aachen, Germany
[15]University College London, London WC1E 6BT, UK
[16]Department of Physics, Schuster Laboratory, The University, Manchester M13 9PL, UK
[17]Department of Physics, University of Maryland, College Park, MD 20742, USA
[18]Laboratoire de Physique Nucléaire, Université de Montréal, Montréal, Quebec H3C 3J7, Canada
[19]University of Oregon, Department of Physics, Eugene OR 97403, USA
[20]Rutherford Appleton Laboratory, Chilton, Didcot, Oxfordshire OX11 0QX, UK
[22]Department of Physics, Technion-Israel Institute of Technology, Haifa 32000, Israel
[23]Department of Physics and Astronomy, Tel Aviv University, Tel Aviv 69978, Israel
[24]International Centre for Elementary Particle Physics and Department of Physics, University of Tokyo, Tokyo 113, and Kobe University, Kobe 657, Japan
[25]Brunel University, Uxbridge, Middlesex UB8 3PH, UK
[26]Particle Physics Department, Weizmann Institute of Science, Rehovot 76100, Israel
[27]Universität Hamburg/DESY, II Institut für Experimental Physik, Notkestrasse 85, D-22607 Hamburg, Germany
[28]University of Victoria, Department of Physics, P O Box 3055, Victoria BC V8W 3P6, Canada

[29]University of British Columbia, Department of Physics, Vancouver BC V6T 1Z1, Canada
[30]University of Alberta, Department of Physics, Edmonton AB T6G 2J1, Canada
[31]Duke University, Dept of Physics, Durham, NC 27708-0305, USA
[32]Research Institute for Particle and Nuclear Physics, H-1525 Budapest, P O Box 49, Hungary
[33]Institute of Nuclear Research, H-4001 Debrecen, P O Box 51, Hungary
[34]Ludwigs-Maximilians-Universität München, Sektion Physik, Am Coulombwall 1, D-85748 Garching, Germany

[a] and at TRIUMF, Vancouver, Canada V6T 2A3
[b] and Royal Society University Research Fellow
[c] and Institute of Nuclear Research, Debrecen, Hungary
[d] and Department of Experimental Physics, Lajos Kossuth University, Debrecen, Hungary

1 Introduction

We present measurements of cross-sections and forward-backward asymmetries in e^+e^- collisions at a centre-of-mass energy, $\sqrt{s}$, of 161 GeV. The data were recorded by the OPAL experiment at LEP in July and August 1996. These are the first e^+e^- collision data available at energies above the W^+W^- production threshold. Cross-sections were measured for multihadronic, $b\overline{b}$, e^+e^-, $\mu^+\mu^-$, and $\tau^+\tau^-$ final states, and the forward-backward asymmetries for the leptonic final states were obtained.

The analyses presented here are similar to those performed at centre-of-mass energies between 130 and 140 GeV [1]. A feature of e^+e^- collision data at energies well above the Z^0 mass is a tendency for radiative return to the Z^0. If one or more initial-state radiation photons are emitted which reduce the effective centre-of-mass energy of the subsequent e^+e^- collision, $\sqrt{s'}$, to the region of the Z^0 resonance, the cross-section is greatly enhanced. Separation between radiative events and those with $\sqrt{s'} \sim \sqrt{s}$ was performed using methods similar to the 130–140 GeV analyses. The isolation of events with $\sqrt{s'} \sim \sqrt{s}$ allows a comparison of the Standard Model with data at the highest e^+e^- energies.

The comparable size of the photon-exchange and Z^0-exchange amplitudes in the non-radiative data at 161 GeV allows constraints to be placed on the size of the interference terms between γ and Z^0 amplitudes, complementing measurements on the Z^0 peak. In this paper we also use the data to place limits on possible contributions from extensions of the Standard Model described by effective four-fermion contact interactions.

2 Data and Simulation

The OPAL detector, trigger and data acquisition system are fully described elsewhere [2–6]. The data used in this analysis were recorded at an e^+e^- centre-of-mass energy of 161.3 ± 0.2 GeV [7] and correspond to an integrated luminosity of approximately 10.0 pb^{-1}.

For Monte Carlo simulation studies of $e^+e^- \to$ hadrons we used the PYTHIA5.7 [8] program with input parameters optimized by a study of global event shape variables and particle production rates in Z^0 decay data [9]. For $e^+e^- \to e^+e^-$ we used the BHWIDE [10] Monte Carlo program, and for $e^+e^- \to \mu^+\mu^-$ and $e^+e^- \to \tau^+\tau^-$ the KORALZ4.0 program [11]. Four-fermion backgrounds were modelled with the EXCALIBUR [12] and grc4f [13] generators, with PYTHIA used to check the separate contributions from WW, Zee and Weν diagrams. Two-photon background processes were simulated using PYTHIA and PHOJET [14] at low Q^2, TWOGEN [15], PYTHIA, and HERWIG [16] at high Q^2, and the Vermaseren generator [17] for leptonic final states. The $e^+e^- \to \gamma\gamma$ background in the e^+e^- final state was modelled with the RADCOR [18] program, while the contribution from $e^+e^-\gamma$ where the photon and one of the charged particles is inside the detector acceptance was modelled with TEEGG [19]. All samples were processed through the OPAL detector simulation [20].

3 Measurement of the Luminosity

The luminosity was measured using small-angle Bhabha scattering events, $e^+e^- \to e^+e^-$, recorded in the silicon-tungsten luminometer [4]. Bhabha events were selected by requiring

a high energy cluster in each end of the detector, using asymmetric acceptance cuts. The main change with respect to the previous analysis at 130–140 GeV centre-of-mass energy [1] results from the introduction of tungsten shields, placed symmetrically on both sides of the interaction region, which are designed to protect the central tracking detectors from synchrotron radiation. The shields, 5 mm thick and 334 mm long, present roughly 50 radiation lengths to particles originating from the interaction region, almost completely absorbing electromagnetically showering particles between 26 mrad and 33 mrad from the beam axis. The fiducial regions for accepting Bhabha events were therefore reduced, to between 38 and 51 mrad on one side, and between 34 and 55 mrad on the opposite side. The Monte Carlo program BHLUMI4.3 was used to calculate the Bhabha cross-section [21]. The Monte Carlo predicts the ratio between the new and old acceptance cuts to be 0.4628 ± 0.0004. Comparing with data taken at centre-of-mass energies around 91 GeV and 133 GeV, agreement within the statistical errors of 0.05% and 0.5% respectively has been found, giving confidence in our understanding of the acceptance.

The relative error on the luminosity measurement obtained was 0.58%, dominated by statistics in the data (0.42%), theoretical knowledge of the cross-section (0.25%), and uncertainty in the beam energy (0.25%).

A second luminosity measurement was available from the lead-scintillator sampling calorimeter (forward detector) covering the region 60 to 150 mrad from the beam axis. The selection of Bhabha events within the calorimeter acceptance was identical to that used in the analysis at 130–140 GeV [1]. The overall acceptance of the calorimeter was measured by normalizing to the precisely known cross-section for hadronic events at the Z^0 peak, using data collected during the calibration run immediately preceding the 161 GeV data-taking. The systematic error on this luminosity measurement amounts to 1.9%, arising mainly from the statistical precision of the acceptance normalization. The integrated luminosity measured by the forward detector agreed with that measured by the silicon-tungsten luminometer to 0.6%, which is less than one standard deviation of the combined statistical error.

A further check of the luminosity was made using Bhabha scattering events recorded in the electromagnetic calorimeter, as described in section 5. Using events within the region $|\cos\theta| < 0.96$, where θ is the polar angle with respect to the electron beam direction, the luminosity measurement has been checked with a statistical precision of 1.6%.

4 Hadronic Events

Hadronic events were selected from the data using the same criteria as in earlier OPAL studies of hadronic Z^0 decays [22], with some small modifications to the cuts. As in the 130–140 GeV analysis [1] the cut on scaled visible energy ($R_{\rm vis} \equiv \Sigma E_{\rm clus}/\sqrt{s}$, where all cluster energies $E_{\rm clus}$ in the lead glass calorimeters are summed) was tightened from 0.10 to 0.14 in order to reduce the background from two-photon processes. In addition, the cut on the momentum imbalance in the beam direction, defined as $R_{\rm bal} \equiv \mid \Sigma(E_{\rm clus}\cos\theta_{\rm clus}) \mid /\Sigma E_{\rm clus}$, where $\theta_{\rm clus}$ is the polar angle of the cluster, and the sum runs over all clusters, was loosened from 0.65 to 0.75 in order to accept more efficiently the events where high energy initial state photons escape close to the beam line. With these cuts we achieve an efficiency of $(92.6\pm0.2)\%$ for events with an effective centre-of-mass energy $\sqrt{s'} > 0.1\sqrt{s}$. This inclusive sample includes events with an additional low mass fermion pair arising from virtual photon radiation.

Background from W pair production, Weν and Zee processes was subtracted; this was estimated to contribute 4.4 ± 0.4 pb as predicted by PYTHIA, 3.3 pb of which arises from W pair production. The error is dominated by the uncertainties of the centre-of-mass energy and of the W mass. The two-photon background has been obtained comparing the predictions of all generators mentioned above and amounts to 1.9 ± 1.0 pb, where the error covers the range of predictions obtained from models compatible with the data. The number of events observed, and the corresponding cross-section after background subtraction and correction for efficiency, are shown in table 1.

The uncertainty on the cross-section is dominated by the statistics of the selected multi-hadron sample. The main systematic uncertainties come from detector simulation uncertainties (1.0%) and from knowledge of the two-photon background contamination (0.7%). The uncertainty from W pair background events is negligibly small.

The effective centre-of-mass energy, $\sqrt{s'}$, of the e^+e^- collision was estimated as follows. Isolated photons in the electromagnetic calorimeter were identified, and the remaining particles were formed into jets. The energy carried by additional photons emitted close to the beam directions was estimated by performing kinematic fits assuming zero, one or two such photons. The value of $\sqrt{s'}$ was then computed from the fitted momenta of the jets, i.e. excluding photons identified in the detector or close to the beam directions. As a systematic check, the simpler method described in [23] was used, which allowed for just single photon radiation, and consistent results were obtained.

By making a cut on the reconstructed value of $\sqrt{s'}$, the cross-section for 'non-radiative' events with only a little initial-state radiation can be derived. We take $s'/s > 0.8$ to define this sample. The efficiency of the selection for these non-radiative events was predicted from the simulation to be 91.8%, with a purity of 94.8% of selected events having a true ratio of $s'/s > 0.8$. The principal background is an estimated 2.6 pb arising from four-fermion (mainly W pair) events[1]. The cross-section, after correction for acceptance, resolution and background, is again shown in table 1. The total and non-radiative cross-sections are shown in figure 1.

In the non-radiative sample, the main systematic uncertainty arises from the modelling of the separation of the radiative and non-radiative events, estimated to be at the level of 2.0% by comparing different separation methods. The uncertainty in the four-fermion contribution amounts to 0.7% of the non-radiative cross-section.

5 e^+e^- Final State

Due to the presence of the dominant t-channel diagram, a definition of s' as in the other final states is not meaningful for $e^+e^- \to e^+e^-$. Events with little radiation were therefore selected by a cut on $\theta_{\rm acol}$, the acollinearity angle between electron and positron. An cut of $\theta_{\rm acol} < 10^\circ$ roughly corresponds to a cut on the effective centre-of-mass energy of $s'/s > 0.8$, for the s-channel contribution. Events with this acollinearity angle cut and the observed electron in the polar angle range $|\cos\theta_{e^-}| < 0.7$ were selected using the same criteria as at 130–140 GeV [1], except that the cut on minimum total electromagnetic calorimeter energy was reduced from 80% to 50% of the centre-of-mass energy. The background in the selected events is estimated

[1] In contrast to the inclusive case, here we subtracted all four-fermion events including those from neutral current production processes, since essentially all of the latter involve radiative return to the Z^0.

	Sel. events	σ (pb)	$\sigma^{\rm SM}$ (pb)
Hadrons ($s'/s > 0.01$)	1472	152±4±2	149
Hadrons ($s'/s > 0.8$)	370	35.3±2.0±0.7	33.2
$e^+e^-(\lvert\cos\theta_{e^-}\rvert < 0.7,\ \theta_{\rm acol} < 10^\circ)$	285	28.1±1.7±0.2	28.1
$e^+e^-(\lvert\cos\theta\rvert < 0.9,\ \theta_{\rm acol} < 170^\circ)$	1582	158±4±2	153
$e^+e^-(\lvert\cos\theta\rvert < 0.96,\ \theta_{\rm acol} < 10^\circ)$	4447	435±7±6	424
$\mu^+\mu^-(s'/s > 0.01)$	98	12.5±1.2±0.5	11.3
$\mu^+\mu^-(s'/s > 0.8)$	44	4.6±0.7±0.2	4.5
$\tau^+\tau^-(s'/s > 0.01)$	64	15.7±2.0±0.7	11.3
$\tau^+\tau^-(s'/s > 0.8)$	43	6.7±1.0±0.3	4.5
Heavy Quark Rates	Sel. hemisph.	$R_{\rm q}$	$R_{\rm q}^{\rm SM}$
$b\bar{b}(s'/s > 0.8)$	76 − 24	0.141±0.028±0.012	0.168

Table 1: Numbers of events and measured cross-sections at $\sqrt{s}$=161.3 GeV. For the cross-sections, the first error shown is statistical, the second systematic. The systematic errors include a common contribution of 0.58% from the luminosity determination, 0.25% of which results from the uncertainty in the centre-of-mass energy. The last column shows the Standard Model cross-section predictions from ZFITTER [24] (hadrons, $\mu^+\mu^-$, $\tau^+\tau^-$, $R_{\rm b}$) and ALIBABA [25] (e^+e^-). As in ref. [1], the measured cross-sections are corrected to the phase-space limit imposed by the s'/s cut with s' defined as the invariant mass of the outgoing two-fermion system *before* final-state photon radiation. There is a small ambiguity associated with this definition, coming from the effect of interference between initial- and final-state radiation, but this is estimated to be small compared to the precision of the measurements.

to amount to 0.36±0.12 pb, arising mainly from $\tau^+\tau^-$ pairs. The number of events selected and the corresponding cross-section are shown in table 1, and compared with the Standard Model prediction in figure 1. The systematic error on this selection is estimated to be 0.6%, dominated by knowledge of inefficiency (0.5%) in the selection.

A more inclusive sample of events was selected by loosening the acollinearity angle cut to 170° and requiring that both electron and positron be observed within $|\cos\theta| < 0.9$. The background in this sample, arising mainly from $\tau^+\tau^-$ and two-photon events, was estimated to be 2.3±0.7 pb. The observed number of events and resulting cross-section for this inclusive selection are shown in table 1. Finally, a large acceptance selection over the extended range $|\cos\theta| < 0.96$, with $\theta_{\rm acol} < 10^\circ$, has been made, using the criteria employed at 130–140 GeV [1]. This selection makes no explicit requirements that there be tracks associated to the electromagnetic clusters, and thus includes (3.1±0.1)% background from the $\gamma\gamma$ final state. The main systematic uncertainty arises from how well the edge of the acceptance is modelled, determined by comparing measurements of polar angle in the electromagnetic calorimeter with those measured in the central tracking chambers and muon detectors. The observed number of events and cross-section are shown in table 1; the cross-section predicted by the ALIBABA [25] program is also shown in the table. This selection is dominated by the t-channel process, therefore the agreement between data and prediction provides a further consistency check of the measured luminosity.

The forward-backward asymmetry for the 'non-radiative' sample within the angular range $|\cos\theta_{e^-}| < 0.7$ was evaluated with a counting method, summing the number of events in the

forward and backward $\cos\theta_{e^-}$ hemispheres. The measured value of 0.88 ± 0.03 is compared with measurements at the Z^0 peak and at 130–136 GeV in figure 2(a), and with the prediction of ALIBABA. Figure 2(c) shows the angular distribution of the scattered electron, compared with the expectation from BHWIDE.

6 $\mu^+\mu^-$ and $\tau^+\tau^-$ Final States

The selection of $\mu^+\mu^-$ events followed that described in previous publications [1, 26], and is estimated to have an efficiency of $(75.6\pm0.2)\%$ for events with $s'/s > 0.01$, and $(89.4\pm0.2)\%$ for events with $s'/s > 0.8$. The value of s' was estimated event-by-event from the polar angles of the two muons relative to the beam axis, as at 130–140 GeV [1]. As for the hadronic event sample, a 'non-radiative' event sample was selected by requiring that the reconstructed s' satisfy $s'/s > 0.8$. Corrections were applied for the inefficiency of this selection, background contamination, and the feed-through of $(5.6\pm0.2)\%$ from lower s'/s values. Background from other processes was estimated to be 0.11 ± 0.02 pb and 0.47 ± 0.06 pb for the non-radiative and inclusive samples, respectively, where the dominant sources are $e^+e^- \to \tau^+\tau^-$ and $e^+e^- \to e^+e^-\mu^+\mu^-$ events. The numbers of selected events, and the cross-sections derived, are shown in table 1. Statistical errors are dominant over the systematic ones, which mainly come from background uncertainties.

The forward-backward asymmetry was evaluated from the observed $\cos\theta$ of the μ^-, using a counting method. Monte Carlo events were used to correct for efficiency and background, including feed-through of muon pair events with lower s'/s into the non-radiative sample. The asymmetries obtained, corrected to the full acceptance, are 0.15 ± 0.11 for the full sample ($s'/s > 0.01$) and 0.49 ± 0.14 for the non-radiative events ($s'/s > 0.8$), where in each case the error is dominated by statistics. The angular distribution of the μ^- is shown in figure 2(d), manifesting the expected asymmetry.

An inclusive sample of $\tau^+\tau^-$ events was selected using the cuts described in [22], after loosening the acollinearity angle cut to $\theta_{\rm acol} < 90^\circ$, and in addition placing requirements on observed total energy and momentum similar to those used in the analysis at 130–140 GeV [1]. These additional requirements have been modified for 161 GeV centre-of-mass energy as follows. The total visible energy in the event, derived from all track momenta plus the sum of all energy deposited in the electromagnetic calorimeter, was required to exceed $0.32\sqrt{s}$ and to be less than $1.35\sqrt{s}$. The polar angles, $\theta_{\rm miss}$, of the two missing momentum vectors with respect to the beam direction, evaluated firstly using only tracks and secondly only clusters in the electromagnetic calorimeter, were not allowed to exceed values of $|\cos\theta_{\rm miss}|$ of 0.95 and 0.90, respectively. The transverse component of the latter missing momentum, divided by $\sin\theta_{\rm miss}$, had to exceed $0.02\sqrt{s}$. These requirements were found to reduce substantially the large background from two-photon processes. Finally, the acoplanarity angle, defined as $180^\circ - \phi$ where ϕ is the angle between the two τ cones in the plane transverse to the beam direction, had to be less than 30°, and events identified as W pairs according to the criteria in [27] were rejected.

The absolute efficiency of the selection is predicted to be $(37.8\pm0.2)\%$ for events with $s'/s > 0.01$. The residual background in the sample was estimated to be 0.52 ± 0.05 pb, with the dominant contributions from $e^+e^- \to e^+e^-$, $e^+e^- \to \mu^+\mu^-$, and $e^+e^- \to e^+e^-\ell^+\ell^-$. The number of selected events and corresponding measured cross-section are shown in table 1.

The background to $\tau^+\tau^-$ events with $s'/s > 0.8$ is much less problematic than for the inclusive sample, since the signal events are more collinear. The selection of the non-radiative sample was therefore able to proceed with less modification to the criteria of [22] and of [1]. The main changes with respect to the 130–140 GeV analysis were that the total visible energy cut was lowered from $0.35\sqrt{s}$ to $0.28\sqrt{s}$ and the transverse momentum cut was lowered from $0.08\sqrt{s}$ to $0.05\sqrt{s}$. The absolute efficiency of the selection was thereby increased to $(58.7\pm0.3)\%$ at 161 GeV, for events with true $s'/s > 0.8$. The residual background in the sample from other channels, mainly two-photon events, was 0.21 ± 0.03 pb, and the background from lower s'/s was 4.6%. The corresponding measured cross-section is shown in table 1 and figure 1.

The distribution of $\cos\theta$ for the τ^- is shown in figure 2(e). The forward-backward asymmetry is measured in these τ-pair events using a counting method, correcting for acceptance and background as for the muon channel. The result for the inclusive sample is 0.40 ± 0.13, and 0.52 ± 0.14 for the $s'/s > 0.8$ sample, where the errors are dominated by statistics.

Combined asymmetries from the $\mu^+\mu^-$ and $\tau^+\tau^-$ channels were obtained, assuming μ-τ universality, by forming a weighted average of the corrected numbers of forward and backward events observed in the two channels. A combined asymmetry of 0.25 ± 0.08 was obtained for the sample with $s'/s > 0.01$ and 0.51 ± 0.09 for $s'/s > 0.8$, as shown in figure 2(b).

7 The Fraction R_{b} of $\mathrm{b\overline{b}}$ Events

The ratio R_{b} of the cross-section for $\mathrm{b\overline{b}}$ production to the hadronic cross-section has been measured in Z^0 decays with an accuracy of better than 1% [28]. Some measurements have suggested a discrepancy with the Standard Model prediction. A measurement at higher energies might be sensitive to any possible new physics affecting R_{b}.

To measure R_{b} at 161 GeV we have performed b flavour tagging for the multihadronic events with $s'/s > 0.8$, selected as described above, requiring in addition at least seven tracks that pass standard track quality requirements, and θ_{thrust}, the polar angle of the thrust direction, to fulfil $|\cos\theta_{\mathrm{thrust}}| < 0.9$. These additional requirements select a sample of 326 events. Each hadronic event was divided into two hemispheres by the plane perpendicular to the thrust axis, and the hemispheres were examined separately.

The b-tagging technique is based on the relatively long lifetime (~ 1.5 ps) of bottom hadrons, which allows the detection of secondary vertices significantly separated from the primary vertex. The primary vertex for each event was reconstructed using a χ^2 minimization method incorporating the average beam spot position, determined from tracks and the LEP beam orbit measurement system, as a constraint. Although the beam spot is less precisely determined than at LEP 1, the resulting error on the primary vertex position is still small compared to the errors on the reconstructed secondary vertex positions. The secondary vertex reconstruction was the same as adopted in [29], but the minimum number of tracks forming a vertex was reduced from four to three. For each reconstructed secondary vertex, the decay length L was defined as the distance of the secondary vertex from the primary vertex in the plane transverse to the beam direction. The sign of the decay length was taken to be $L > 0$ if the secondary vertex was displaced from the primary vertex in the same hemisphere as the momentum sum of the charged particles at the vertex, and $L < 0$ otherwise. Each event hemisphere was assigned a vertex tag if it contained at least one secondary vertex with a signed decay length significance (defined as the signed decay length L divided by its error σ_L) greater than three. The

decay length significance distribution is shown in figure 3(a), superimposed on the Monte Carlo simulation. Possible systematic effects arising from deficiencies in the simulation of the decay length distribution have been assessed by considering data taken on the Z^0 peak, as described below.

A "folded tag" was used in this analysis, in order to reduce the sensitivity to detector resolution uncertainties and the light flavour component. In this method, the background from light quark decays with $L/\sigma_L > 3$ is accounted for by subtracting the number of hemispheres with $L/\sigma_L < -3$. The folded tag is fully described in [29]. Neglecting background in the hadronic sample, the difference between the number of forward ($L/\sigma_L > 3$) and backward ($L/\sigma_L < -3$) tagged hemispheres $N_t - \overline{N}_t$ in a sample of N_{had} hadronic events can be expressed as:

$$N_t - \overline{N}_t = 2N_{had}[(\epsilon_{\rm b} - \overline{\epsilon}_{\rm b})R_{\rm b} + (\epsilon_{\rm c} - \overline{\epsilon}_{\rm c})R_{\rm c} + (\epsilon_{\rm uds} - \overline{\epsilon}_{\rm uds})(1 - R_{\rm b} - R_{\rm c})] \qquad (1)$$

where $(\epsilon_{\rm b} - \overline{\epsilon}_{\rm b})$, $(\epsilon_{\rm c} - \overline{\epsilon}_{\rm c})$ and $(\epsilon_{\rm uds} - \overline{\epsilon}_{\rm uds})$ are the differences between the forward and backward tagging efficiencies, and $R_{\rm c}$ is the ratio of the cross-section for $\rm c\overline{c}$ production to the hadronic cross-section. $R_{\rm c}$ was computed using ZFITTER, and found to be $R_{\rm c} = 0.245$. The hemisphere tagging efficiency differences were determined from Monte Carlo, and found to be $(\epsilon_{\rm b} - \overline{\epsilon}_{\rm b}) = 0.403 \pm 0.022$, $(\epsilon_{\rm c} - \overline{\epsilon}_{\rm c}) = 0.082 \pm 0.007$ and $(\epsilon_{\rm uds} - \overline{\epsilon}_{\rm uds}) = 0.0083 \pm 0.0004$, where the last is a weighted average of the light quarks. The errors include Monte Carlo statistics and systematic effects, the latter being dominant. From Monte Carlo simulation the b-tagged event sample was estimated to be 74% $\rm b\overline{b}$, 21% $\rm c\overline{c}$, and 5% light flavour events. The expected contribution from W pair events was subtracted, as described above for the multihadronic events. The probability for a W pair event to be b-tagged was estimated from Monte Carlo to be 8.2%.

In the 326 non-radiative hadronic events, 76 forward and 24 backward tagged hemispheres were found. We obtain

$$R_{\rm b}(\sqrt{s} = 161\,{\rm GeV}) = 0.141 \pm 0.028 \pm 0.012$$

where the first error is statistical and the second systematic. The systematic errors on $R_{\rm b}$ arising from uncertainties in the b and c fragmentation and decay parameters were estimated by following the prescriptions of [28]. The other important systematics result from Monte Carlo statistics and detector resolution. To check modelling of the detector resolution, the analysis was repeated on data collected at the Z^0 peak immediately before the 161 GeV data-taking. The result was $(5.5 \pm 2.1)\%$ below the OPAL measurement [29]; the difference of 5.5% was included in the systematic error.

We also applied this analysis to OPAL data collected at the end of 1995 at centre-of-mass energies of 130 GeV and 136 GeV. The average centre-of-mass energy was $\sqrt{s} = 133$ GeV. The event selection and b-tagging procedures were the same as used for the 161 GeV data, except that the cut $|\cos\theta_{\rm thrust}| < 0.8$ was used instead of $|\cos\theta_{\rm thrust}| < 0.9$ due to the different geometry of the microvertex detector in 1995. In total 257 non-radiative hadronic events were selected. Within this sample, 69 forward and 13 backward tagged hemispheres were found. The hemisphere tagging efficiency differences were determined to be $(\epsilon_{\rm b} - \overline{\epsilon}_{\rm b}) = 0.409 \pm 0.022$, $(\epsilon_{\rm c} - \overline{\epsilon}_{\rm c}) = 0.075 \pm 0.007$ and $(\epsilon_{\rm uds} - \overline{\epsilon}_{\rm uds}) = 0.0070 \pm 0.0007$. The fractions of tagged $\rm b\overline{b}$ and $\rm c\overline{c}$ events in the sample were 79% and 17% respectively. The higher b purity, compared to 161 GeV, is caused by the higher ratio $R_{\rm b}/R_{\rm c}$. The value $R_{\rm c} = 0.225$ at 133 GeV was determined using ZFITTER. We find

$$R_{\rm b}(\sqrt{s} = 133\,{\rm GeV}) = 0.216 \pm 0.034 \pm 0.013$$

where the first error is statistical and the second systematic.

The results for both centre-of-mass energies are compared to the Standard Model prediction in figure 3(b), where $R_{\rm b}$ is plotted as a function of $\sqrt{s}$.

8 Influence on Electroweak Precision Measurements

The cross-section and asymmetry measurements presented here are all consistent with the Standard Model expectations, as illustrated in figures 1-2 and table 1.

In ref. [1] we showed that non-radiative data above the Z^0 resonance can be used to constrain the size of the interference terms between photon-exchange and Z^0-exchange processes, which have amplitudes of similar magnitude. Using the ZFITTER [24] and SMATASY [30] programs, we have repeated the model-independent fit to OPAL data described in ref. [1], including the measurements of the non-radiative multihadron cross-section and combined $\mu^+\mu^-$ and $\tau^+\tau^-$ asymmetry presented here. In the fit, the parameters $j^{\rm tot}_{\rm had}$ and $j^{\rm fb}_\ell$, determining the sizes of the hadronic and leptonic γZ^0-interference, respectively, have been left free (see ref. [1] for more discussion of these parameters and details of the fit). In the Standard Model, $j^{\rm tot}_{\rm had}$ and $j^{\rm fb}_\ell$ have the values 0.22 and 0.799 respectively, for a top quark mass of 180 GeV and Higgs boson mass of 300 GeV. The results of the fit are given in table 2, where the errors of the ZFITTER prediction at the various values of s have been taken into account. For comparison, the table also shows the results of the fits presented in [1] to LEP 1 data alone and to LEP 1 data plus non-radiative multihadron cross-sections and combined $\mu^+\mu^-$ and $\tau^+\tau^-$ asymmetries at 130 and 136 GeV. Since the γZ^0-interference vanishes on the Z^0 peak, the inclusion of data far away from the Z^0 resonance considerably reduces the uncertainty of $j^{\rm tot}_{\rm had}$ [1]. The inclusion of the 130 and 136 GeV data reduced the uncertainty on $j^{\rm tot}_{\rm had}$ by 40%; a further improvement of about 25% is observed by including the data presented here. As shown in ref. [1], this improvement is much larger than that which would be obtained by the inclusion of the full LEP 1 off-peak data. The high energy data also reduce the correlation between fitted values of $j^{\rm tot}_{\rm had}$ and the Z^0 mass, as can be seen in table 2 and figure 4.

OPAL data sample	$j^{\rm tot}_{\rm had}$	$m_{\rm Z}$ (GeV)	$j^{\rm tot}_{\rm had}$, $m_{\rm Z}$ correlation	$j^{\rm fb}_\ell$
LEP 1 (1989-92) [22,26,31]	-0.18 ± 0.68	91.187 ± 0.013	-0.70	0.684 ± 0.053
LEP 1 + 130–136 GeV [1]	-0.53 ± 0.41	91.192 ± 0.011	-0.50	0.717 ± 0.048
LEP 1 + 130–136 GeV + 161 GeV	-0.05 ± 0.31	91.185 ± 0.010	-0.41	0.713 ± 0.045

Table 2: Fitted values of the hadronic γZ^0-interference parameter, $j^{\rm tot}_{\rm had}$, the Z^0 mass, $m_{\rm Z}$, and the leptonic γZ^0-interference parameter, $j^{\rm fb}_\ell$, using different OPAL data samples. The $m_{\rm Z}$ values are quoted for the s-dependent Z^0-width.

9 Limits on Four-fermion Contact Interactions

In ref. [32] we used our data at 130–136 GeV [1] to place limits on possible four-fermion contact interactions. The basic idea is that the Standard Model could be part of a more general theory

characterized by an energy scale Λ. The consequences of the theory would be observed at energies well below Λ as a deviation from the Standard Model which could be described by an effective contact interaction. In the context of composite models of leptons and quarks, the contact interaction is regarded as a remnant of the binding force between the substructure of fermions. If electrons were composite, such an effect would appear in Bhabha scattering ($e^+e^- \to e^+e^-$). If the other leptons and quarks shared the same type of substructure, the contact interaction would exist also in the processes $e^+e^- \to \mu^+\mu^-$, $e^+e^- \to \tau^+\tau^-$ and $e^+e^- \to q\overline{q}$. More generally, the contact interaction is considered to be a convenient parametrization to describe possible deviations from the Standard Model which may be caused by some new physics.

It is expected that the sensitivity of the measurements to the contact interaction will increase with centre-of-mass energy ($\sqrt{s}$) due to the decrease of the Standard Model cross-section as $1/s$. Therefore we have repeated the contact interaction analysis of ref. [32] including the data presented here on the angular distributions for the non-radiative $e^+e^- \to e^+e^-$, $e^+e^- \to \mu^+\mu^-$, $e^+e^- \to \tau^+\tau^-$ processes, the cross-section for $e^+e^- \to q\overline{q}$, and the measurements of R_b. The only new feature in the analysis is the inclusion of R_b. The results are shown in Table 3, where the notation is identical to ref. [32]. We see that the inclusion of the 161 GeV data has increased the sensitivity factor λ [32] by typically 1 TeV, and the limits on Λ are generally close to the sensitivity estimate. As before, the data are particularly sensitive for the VV and AA models; the combined data give limits on Λ in the range 5.0–6.5 TeV for these models, roughly 1 TeV higher than those for 130–136 GeV data alone. The limits for the other models lie in the range 2.6–4.0 TeV, approximately 0.7 TeV above those from previous data.

10 Conclusion

Production of events with two-fermion multihadronic and leptonic final states has been measured in e^+e^- collisions at a centre-of-mass energy of 161 GeV, as summarized in table 1. The measured rates and distributions are all consistent with the Standard Model expectations. From the number of events with a significantly displaced secondary vertex we derive R_b with a 20% statistical error. In a model-independent fit to the Z^0 lineshape, the hadronic cross-section presented here provides a constraint on the size of the interference between Z^0 and photon exchange complementary to that given by LEP 1 data. We have also used these data to place limits on possible deviations from the Standard Model represented by effective four-fermion contact interactions.

Channel	Model	ε (TeV^{-2})	λ (TeV)	Λ^- (TeV)	Λ^+ (TeV)
$e^+e^- \to e^+e^-$	VV	$-0.012^{+0.022}_{-0.022}$	5.3	4.4	5.3
	AA	$-0.007^{+0.038}_{-0.053}$	3.8	2.2	4.0
	LL	$-0.069^{+0.095}_{-0.085}$	2.6	2.2	2.4
	RR	$-0.067^{+0.096}_{-0.086}$	2.6	2.2	2.4
	LR	$-0.021^{+0.069}_{-0.057}$	3.2	2.9	2.5
$e^+e^- \to \mu^+\mu^-$	VV	$0.034^{+0.030}_{-0.030}$	4.5	5.0	3.4
	AA	$-0.006^{+0.036}_{-0.035}$	4.2	3.8	3.7
	LL	$0.051^{+0.073}_{-0.074}$	2.9	2.9	2.4
	RR	$0.054^{+0.079}_{-0.082}$	2.8	2.6	2.3
	LR	$0.103^{+0.078}_{-0.088}$	2.7	1.6	2.1
$e^+e^- \to \tau^+\tau^-$	VV	$0.053^{+0.037}_{-0.036}$	4.1	4.8	2.9
	AA	$0.076^{+0.057}_{-0.053}$	3.3	4.2	2.4
	LL	$0.147^{+0.085}_{-0.086}$	2.7	3.0	1.9
	RR	$0.161^{+0.090}_{-0.093}$	2.6	2.8	1.8
	LR	$0.067^{+0.108}_{-0.368}$	2.2	1.4	2.0
$e^+e^- \to \ell^+\ell^-$	VV	$0.014^{+0.016}_{-0.016}$	6.2	6.6	4.9
	AA	$0.011^{+0.023}_{-0.023}$	5.2	5.0	4.4
	LL	$0.053^{+0.051}_{-0.051}$	3.5	3.8	2.7
	RR	$0.055^{+0.055}_{-0.055}$	3.3	3.6	2.6
	LR	$0.032^{+0.060}_{-0.059}$	3.2	3.2	2.7
$e^+e^- \to q\overline{q}$	VV	$-0.051^{+0.175}_{-0.031}$	4.1	3.3	2.9
	AA	$0.034^{+0.033}_{-0.188}$	3.9	2.8	3.5
	LL	$-0.214^{+0.075}_{-0.054}$	3.2	2.1	2.5
	RR	$-0.104^{+0.349}_{-0.064}$	2.8	2.3	2.1
	LR	$-0.126^{+0.334}_{-0.062}$	2.9	2.2	2.1
	RL	$-0.053^{+0.399}_{-0.062}$	2.9	2.6	2.1
$e^+e^- \to b\overline{b}$	VV	$-0.015^{+0.047}_{-0.076}$	3.4	2.2	3.7
	AA	$-0.006^{+0.033}_{-0.034}$	4.3	3.6	4.1
	LL	$-0.012^{+0.055}_{-0.055}$	3.3	2.9	3.1
	RR	$-0.036^{+0.124}_{-0.273}$	1.9	1.6	2.4
	LR	$-0.049^{+0.181}_{-0.181}$	1.6	1.8	2.1
	RL	$0.010^{+0.178}_{-0.108}$	2.2	2.4	1.7
Combined	VV	$0.011^{+0.016}_{-0.015}$	6.3	6.5	5.1
	AA	$0.007^{+0.018}_{-0.020}$	5.7	5.3	5.0
	LL	$0.026^{+0.037}_{-0.038}$	4.0	4.0	3.4
	RR	$0.048^{+0.053}_{-0.057}$	3.3	3.5	2.8
	LR	$0.033^{+0.062}_{-0.068}$	3.0	3.1	2.8
	RL	$0.019^{+0.067}_{-0.054}$	3.2	3.5	2.6

Table 3: Results of the contact interaction fits to the angular distributions for non-radiative $e^+e^- \to e^+e^-$, $e^+e^- \to \mu^+\mu^-$, $e^+e^- \to \tau^+\tau^-$ and the cross-section for $e^+e^- \to q\overline{q}$ at 130–136 GeV [32] and 161 GeV, and the measurements of R_b presented here. The combined results include all leptonic angular distributions, the multihadronic cross-sections and the R_b measurements. ε is the fitted value of $1/\Lambda^2$.

Acknowledgements

We particularly wish to thank the SL Division for the efficient operation of the LEP accelerator at the new energy of $\sqrt{s} = 161$ GeV and for their continuing close cooperation with our experimental group. We thank our colleagues from CEA, DAPNIA/SPP, CE-Saclay for their efforts over the years on the time-of-flight and trigger systems which we continue to use. In addition to the support staff at our own institutions we are pleased to acknowledge the
Department of Energy, USA,
National Science Foundation, USA,
Particle Physics and Astronomy Research Council, UK,
Natural Sciences and Engineering Research Council, Canada,
Israel Science Foundation, administered by the Israel Academy of Science and Humanities,
Minerva Gesellschaft,
Japanese Ministry of Education, Science and Culture (the Monbusho) and a grant under the Monbusho International Science Research Program,
German Israeli Bi-national Science Foundation (GIF),
Bundesministerium für Bildung, Wissenschaft, Forschung und Technologie, Germany,
National Research Council of Canada,
Hungarian Foundation for Scientific Research, OTKA T-016660, and OTKA F-015089.

References

[1] OPAL Collab., G. Alexander et al., Phys. Lett. **B376** (1996) 232.

[2] OPAL Collab., K. Ahmet et al., Nucl. Instrum. Methods **A305** (1991) 275.

[3] P.P. Allport et al., Nucl. Instrum. Methods **A324** (1993) 34;
P.P. Allport et al., Nucl. Instrum. Methods **A346** (1994) 476.

[4] B.E. Anderson et al., IEEE Transactions on Nuclear Science, 41 (1994) 845.

[5] M. Arignon et al., Nucl. Instrum. Methods **313** (1992) 103;
M. Arignon et al., Nucl. Instrum. Methods **333** (1993) 330.

[6] J.T. Baines et al., Nucl. Instrum. Methods **A325** (1993) 271;
D.G. Charlton, F. Meijers, T.J. Smith and P.S. Wells, Nucl. Instrum. Methods **A325** (1993) 129.

[7] LEP Energy Working Group, private communication.

[8] T. Sjöstrand, Comput. Phys. Commun. **82** (1994) 74.

[9] OPAL Collab., G. Alexander et al., Z. Phys. **C69** (1996) 543.

[10] S. Jadach, W. Placzek, and B.F.L. Ward, University of Tennessee preprint, UTHEP-95-1001.

[11] S. Jadach, B.F.L. Ward and Z. Wąs, Comput. Phys. Commun. **79** (1994) 503.

[12] F.A. Berends, R. Pittau and R. Kleiss, Comput. Phys. Commun. **85** (1995) 437.

[13] J. Fujimoto et al., "grc4f: A Four-Fermion Event Generator for e^+e^- collisions", KEK-CP-046, submitted to Comput. Phys. Commun.

[14] R. Engel and J. Ranft, Phys. Rev. **D54** (1996) 4244.

[15] A. Buijs et al., Comput. Phys. Commun. **79** (1994) 523.

[16] G. Marchesini et al., Comput. Phys. Commun. **67** (1992) 465.

[17] J.A.M. Vermaseren, Nucl. Phys. **B229** (1983) 347.

[18] F.A. Berends and R. Kleiss, Nucl. Phys. **B186** (1981) 22.

[19] D. Karlen, Nucl. Phys. **B289** (1987) 23.

[20] J. Allison et al., Nucl. Instrum. Methods **A317** (1992) 47.

[21] S. Jadach, E. Richter-Wąs, B.F.L. Ward and Z. Wąs, Comput. Phys. Commun. **70** (1992) 305.

[22] OPAL Collab., G. Alexander et al., Z. Phys. **C52** (1991) 175.

[23] OPAL Collab., G. Alexander et al., "QCD Studies with e^+e^- Annihilation Data at 130 and 136 GeV", CERN-PPE/96-047, to be published in Zeit. Phys. C.

[24] D. Bardin et al., CERN-TH 6443/92 (May 1992); Phys. Lett. **B255** (1991) 290; Nucl. Phys. **B351** (1991) 1; Z. Phys. **C44** (1989) 493.
We use ZFITTER version 4.9 with default parameters, except `BOXD`=1, and `FINR`=0. The latter ensures that the final state photons are not included in the definition of s', as discussed in the caption of table 1. We have repeated the model-independent fit of section 8 with a preliminary version of ZFITTER 5.0, and obtain consistent results.

[25] W. Beenakker et al., Nucl. Phys. **B349** (1991) 323.

[26] OPAL Collab., R. Akers et al., Z. Phys. **C61** (1994) 19.

[27] OPAL Collab., K. Ackerstaff et al., "Measurement of the mass of the W boson in e^+e^- collisions at $\sqrt{s} = 161$ GeV", CERN PPE/96-141, to be published in Phys. Lett. B.

[28] The LEP Experiments: ALEPH, DELPHI, L3 and OPAL, Nucl. Instrum. Methods **A378** (1996) 101.

[29] OPAL Collab., R. Akers et al., Z. Phys. **C65** (1995) 17.

[30] S. Kirsch and T. Riemann, Comput. Phys. Commun. **88** (1995) 89.

[31] OPAL Collab., P.D. Acton et al., Z. Phys. **C58** (1993) 219.

[32] OPAL Collab., G. Alexander et al., Phys. Lett. **B387** (1996) 432.

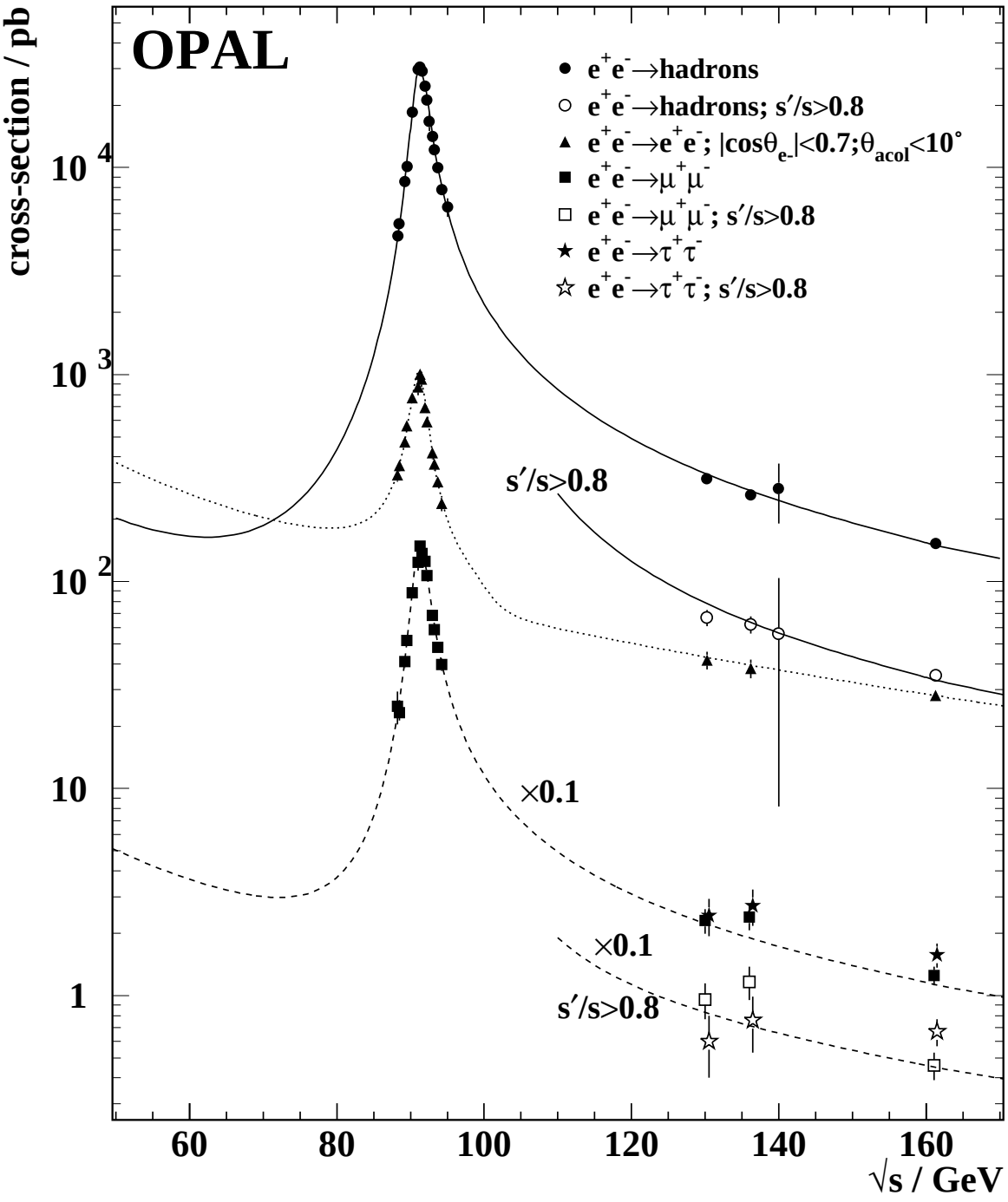

Figure 1: Measured total cross-sections ($s'/s > 0.01$) for different final states at energies around the Z^0 resonance (LEP 1), 130–140 GeV and these data. The cross-sections for $\mu^+\mu^-$ and $\tau^+\tau^-$ production have been reduced by a factor of ten for clarity. The curves show the predictions of ZFITTER for multihadronic (solid), $\mu^+\mu^-$ and $\tau^+\tau^-$ (dashed) final states, that of ALIBABA for the e^+e^- final state (dotted). In the case of multihadrons, muon and tau pairs, cross-section expectations and measurements are shown at high energies also for $s'/s > 0.8$.

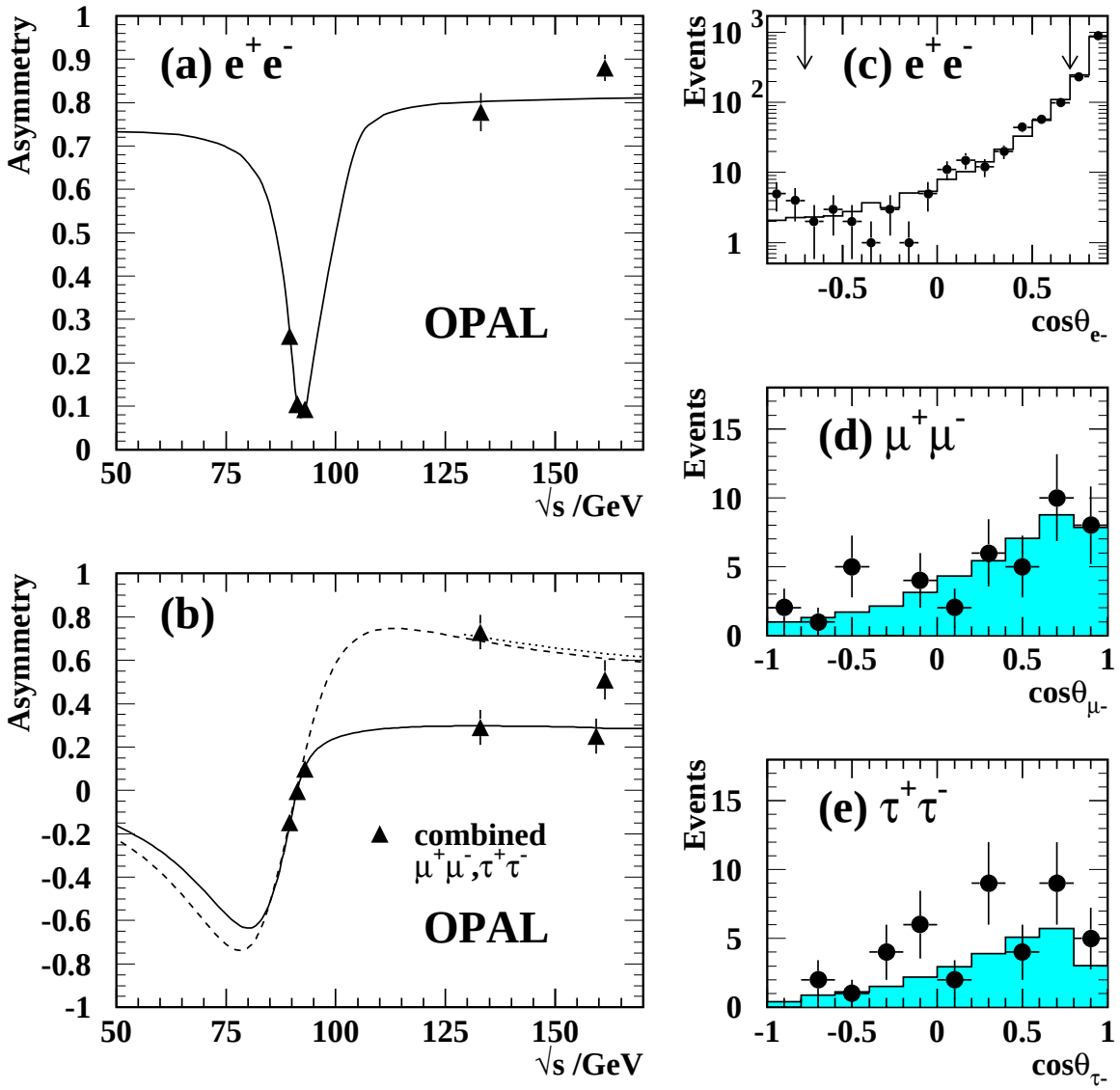

Figure 2: (a) Measured forward-backward asymmetry for electron pairs selected with $|\cos\theta_{e^-}| < 0.7$ and $\theta_{acol} < 10^\circ$, as a function of $\sqrt{s}$. The curve shows the prediction of ALIBABA.
(b) Measured asymmetries for all ($s'/s > 0.01$) and non-radiative ($s'/s > 0.8$) samples as functions of $\sqrt{s}$ for $\mu^+\mu^-$ and $\tau^+\tau^-$ events (combined). The curves show ZFITTER predictions for $s'/s > 0.01$ (solid) and $s'/s > 0.8$ (dotted), as well as the Born-level expectation without QED radiative effects (dashed). The expectation for $s'/s > 0.8$ lies close to the Born curve. The observed distributions of $\cos\theta$ of the outgoing lepton are shown in (c) to (e), for $s'/s > 0.8$ in (d) and (e). The histograms in (c) to (e) show the expected distributions from Monte Carlo simulated events. The arrows in (c) show the positions of the cuts at $|\cos\theta_{e^-}| = 0.7$.

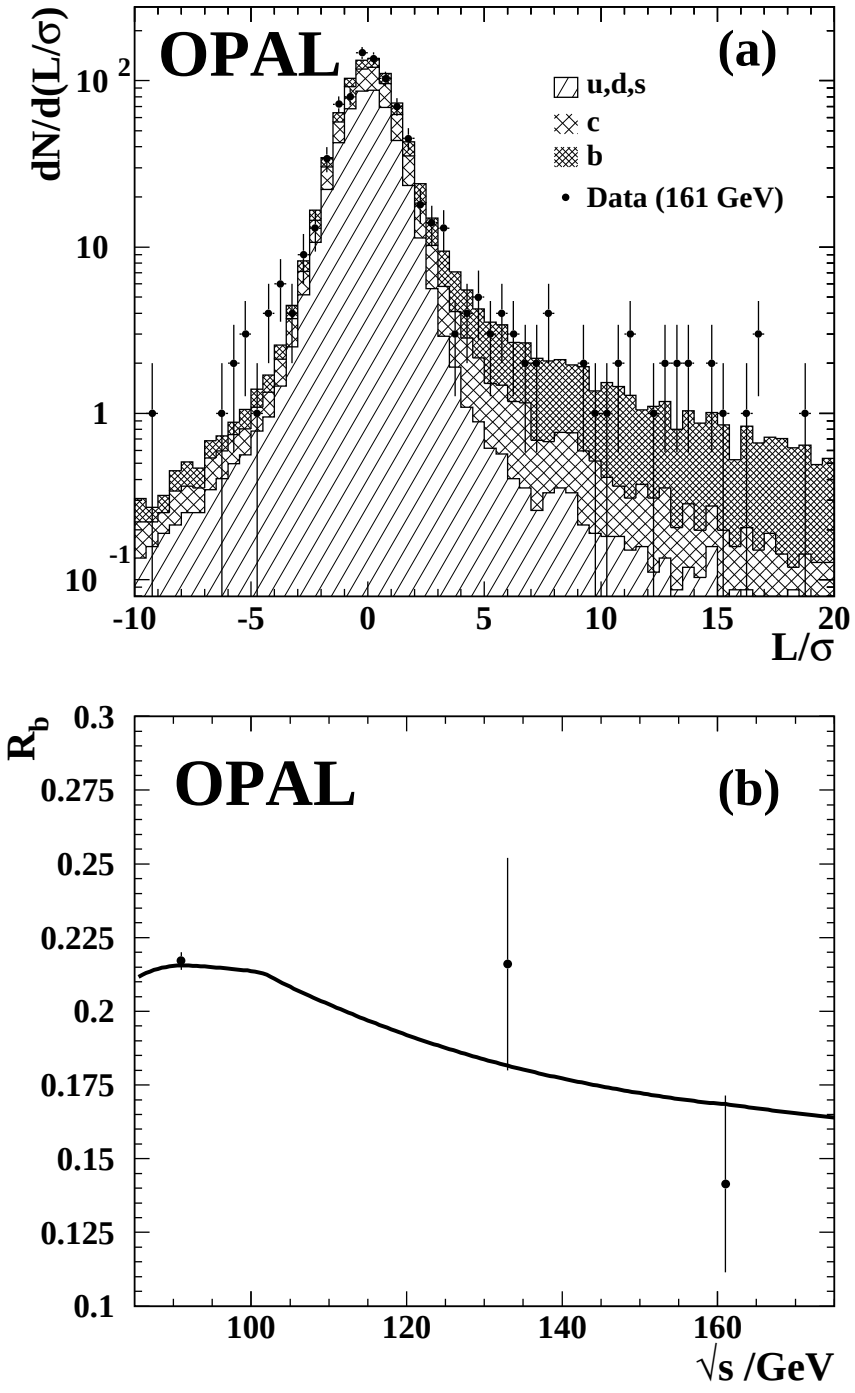

Figure 3: (a) Decay length significance distribution at 161 GeV. The points are the data, and the histograms are the Monte Carlo predictions. (b) R_{b} as a function of the centre-of-mass energy. The points show the measurements presented here, and the value [29] obtained on the Z^0 peak. The errors are statistical and systematic, summed in quadrature. The solid line is the ZFITTER prediction for $s'/s > 0.8$.

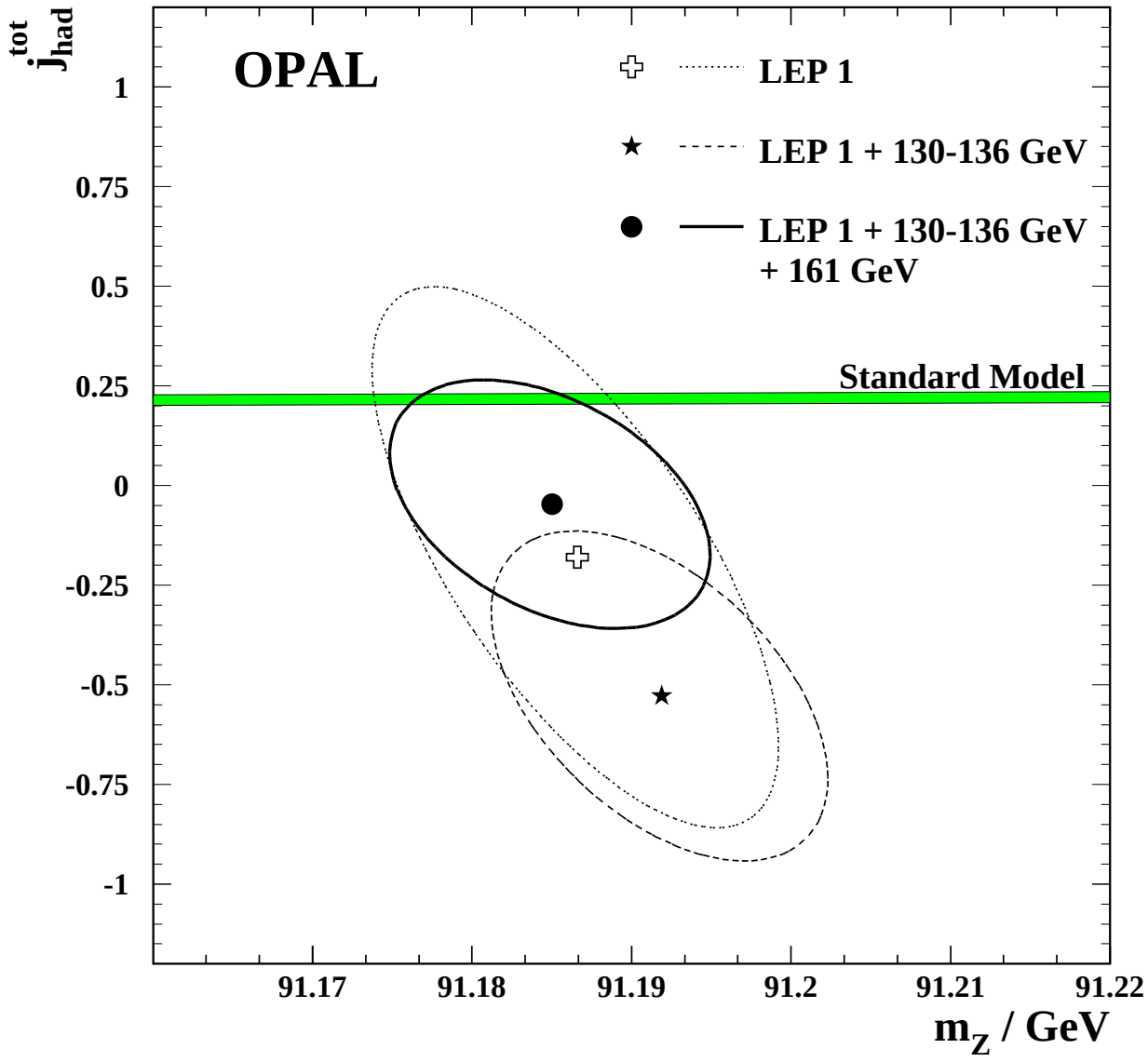

Figure 4: Central values and one standard deviation contours (39% probability content) in the j^{tot}_{had} vs. m_Z plane resulting from model-independent fits to the OPAL data samples described in section 8. The horizontal band shows the Standard Model expectation $j^{tot}_{had} = 0.22 \pm 0.02$ for a top quark mass range of 170-190 GeV and a Higgs mass range of 100-1000 GeV.